ACS APPLIED MATERIALS & INTERFACES

Research Article

www.acsami.org

High Performance of Silicon Nanowire-Based Biosensors using a High-*k* Stacked Sensing Thin Film

Tae-Eon Bae,[†] Hyun-June Jang,[†] Jong-Heon Yang,[‡] and Won-Ju Cho*[,†]

[†]Department of Electronic Materials Engineering, Kwangwoon University, 447-1, Wolgye-dong, Nowon-gu, Seoul 139-701, Korea

[‡]Biosensor Research Team, Electronics and Telecommunications Research Institute (ETRI), Daejeon 305-700, Korea

ABSTRACT: High performance silicon nanowire (SiNW) sensors with $SiO_2/HfO_2/Al_2O_3$ (OHA) engineered sensing thin films were fabricated. A lower interface state density, a larger capacitance and a stronger chemical immunity, which are essential for enhancing the performance of devices, were accomplished by stacking thin SiO_2, HfO_2, and Al_2O_3 layers, respectively, in sequence on the SiNW channel. Compared with the conventional single SiO_2 thin film, the staked OHA thin films demonstrated improved sensing performances; a higher sensitivity, a lower hysteresis voltage, and a smaller drift rate, as well as a higher output current. Therefore, the SiNW sensors with OHA stacked sensing thin films are very promising to biological and chemical sensor applications.

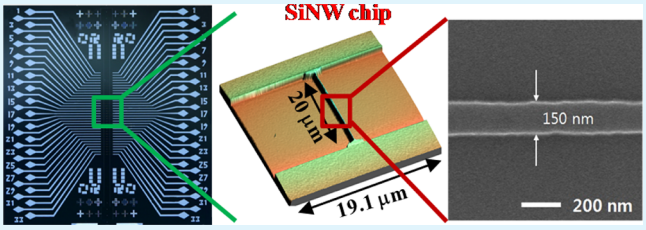

KEYWORDS: *silicon nanowire, biosensor, thin film, $SiO_2/HfO_2/Al_2O_3$ (OHA), sensitivity*

INTRODUCTION

Recently, a number of research groups have explored nanoelectronic sensors for various applications such as disease diagnosis, toxin detection, environmental, and biomedical devices.[1−3] Among them, the silicon nanowire (SiNW) is expected to be a very promising transducer for detecting biological and chemical species in terms of the ultrahigh sensitive, label-free, real-time detection, and CMOS compatibility.[4−7] Especially, Mark Reed group has pioneered the research of SiNW biosensors and has recently expanded this to a number of detection systems and bioapplications including cellular response, specific protein, and DNA recognition assays.[8] Since the conductance of the SiNW channel is easily modulated by a small amount of surface charge induced via protonation or deprotonation processes in the electrolyte, the sensitivity is much higher than the bulk materials.[9] Moreover, the sensing characteristics of SiNW sensors are mainly determined by the inherent properties of the sensing thin film which is in direct contact with the electrolyte. The thermally grown SiO_2 layer first proposed as the sensing thin film of SiNW sensors was used owing to its easy growth, good interface properties as gate insulators, and favorable coupling effects with biomolecules. However, this conventional SiO_2 sensing thin film has been simultaneously exposed to serious damage in chemical aqueous solutions for long-term usage.[10] Thus, over the past few years, as an effort to obtain higher sensitivity and better stability, several materials of metal-oxide with a higher dielectric constant such as Al_2O_3, Er_2O_3, HfO_2, and ZrO_2 have been extensively investigated as sensing thin films of sensors.[11−14] Compared to the thermally grown SiO_2, metal oxides generally show a higher resistance to hydration as well as a high dielectric constant. Nevertheless, each material with a high dielectric constant shows its own limitations in regards to the interface property, long-term stability and memory effect.

In this study, we realized the SiNW sensors using high-*k* stacked $SiO_2/HfO_2/Al_2O_3$ (OHA) engineered sensing thin films to obtain a higher sensitivity, a stronger chemical immunity, and improved reliability for long-term usage. A lower interface state density, a larger capacitance, and a stronger chemical immunity, which are essential for enhancing the performance of devices, were accomplished by stacking thin SiO_2, HfO_2, and Al_2O_3 layers, respectively.[15−17] The sensing characteristics of the engineered OHA thin film were compared with those of the single SiO_2 (O) thin film. As a result, the OHA engineered sensing thin film exhibited much better electrical/chemical stability and performance in comparison with the conventional O thin film.

EXPERIMENTAL SECTION

Measurements. The images of SiNW sensor chips were measured using an atomic force microscopy (AFM) and scanning electron microscopy (SEM). The thickness of each thin film was measured by an ellipsometer. The conductance for the various pH buffer solutions were measured by using a commercial Ag/AgCl reference electrode and Hewlett-Packard 4156B high-precision semiconductor parameter analyzer in a dark box to avoid interference from light and noise.

Device Fabrication. P-type 8 in. silicon-on-insulator (SOI) substrates with a thickness of 100 nm top silicon layer (8.5−22 Ω cm) were used for fabrication of SiNW by the "top-down" method. The initial top Si layer was thinned down to 40 nm by dry oxidation and wet etching, and then implanted with 3×10^{13} cm^{-2} of boron ions at 8 keV to form a p-type channel layer. After activation of implanted

Received: March 22, 2013
Accepted: May 7, 2013
Published: May 7, 2013

   dx.doi.org/10.1021/am401026z | *ACS Appl. Mater. Interfaces* 2013, 5, 5214−5218

boron atoms at 950 °C for 30 min in nitrogen ambient, the SiNW channels of 150−300 nm-widths and 2−20 μm-lengths were prepared to compare the electrical characteristics and sensing properties depending on NW's dimensions. These SiNWs and Si leads were defined by optical lithography using a KrF scanner and dry etching processes. For the ohmic contacts between the Si leads and the metal electrodes, the additional implant of boron with a dose of 2×10^{15} cm^{-2} at the regions of Si leads and the rapid thermal anneal of 950 °C for 30 s were followed. For the OHA stacked sensing thin film, a 5-nm-thick SiO_2 layer was grown by thermal oxidation. Subsequently, a 10-nm-thick HfO_2 layer and a 15-nm-thick Al_2O_3 layer were deposited using atomic layer deposition (ALD). Then, a post deposition anneal (PDA) of high-k layers was carried out by rapid thermal annealing (RTA) at 850 °C for 30 s in a N_2/O_2 gas ambient to reduce the defect density and improve the electrical properties of the devices. For comparison, the single O thin film was prepared by thermal oxidation with a thickness of 30 nm. After deposition of Au/Cr/Al (50 nm/5 nm/50 nm) for metal electrodes, forming gas annealing at 450 °C for 30 min in a 2% H_2/N_2 ambient was carried out to remove the dangling bonds at the interface region. Finally, the reservoir for the injection of the pH buffer solution was mounted on top of SiNW sensors using polydimethylsiloxane (PDMS).

RESULTS AND DISCUSSION

Figure 1a and b show the optical micrographs of fabricated SiNW sensor chips on a 2 cm ×2 cm area. An atomic force

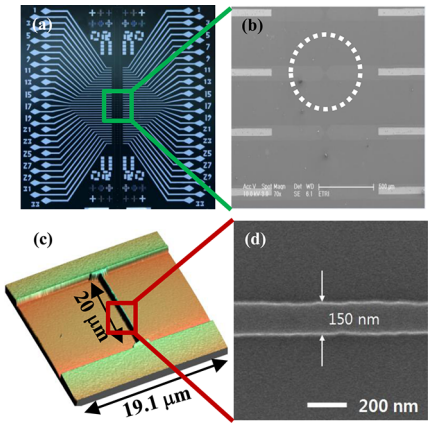

Figure 1. (a) Optical micrographs of a 2 cm ×2 cm single chip containing 33 channels, (b) scanning electron microscopy (SEM) image of a sensing area, (c) atomic force microscopy (AFM) image of a Si nanochannel, (d) magnified SEM image of 150 nm-wide and 20 μm-long SiNW.

microscopy (AFM) image and scanning electron microscopy (SEM) image of a SiNW channel with a 150-nm-width and 20-μm-length are shown in Figure 1c and d, respectively. We confirmed that the dimension of SiNW channels was well controlled from the SEM image. The uniformity of channel dimensions (width and height) was less than ±10% across the 8 in. wafer and the variation of the channel conductance was also within the same range. To obtain a high performance SiNW sensor, the sensing characteristics for many high-*k* dielectric materials were evaluated beforehand using the EIS (electrolyte-insulator-semiconductor) structures. The EIS pH sensors have features of simple structure and easy measurement.[13] Each high-*k* material was deposited on the SiO_2 layer with a good interface property with Si substrate. The pH sensing characteristics of various high-k thin films are summarized in Table 1. It is found that the HfO_2 has the highest dielectric constant and sensitivity among them. However, the main drawback of this

Table 1. pH Sensing Characteristics of All the Sensing Thin Films Based on EIS pH Sensors

sensing thin film	pH sensitivity (mV/pH)	linearity (%)	V_H (mV)	drift rate (mV/h)	dielectric constant
SiO_2 (O)	38.7	99.32	173.0	45.24	3.9
SiO_2/Si_3N_4 (ON)	49.7	99.55	20.9	3.86	7
SiO_2/HfO_2 (OH)	55.3	99.91	6.9	1.88	25
SiO_2/Ta_2O_5 (OT)	52.6	99.51	13.9	0.61	25
SiO_2/ZrO_2 (OZ)	53.9	99.80	22.1	0.44	22
SiO_2/Al_2O_3 (OA)	53.1	99.80	0.6	0.25	9

film is the stability associated with the drift effect and hysteresis phenomenon. On the other hand, the Al_2O_3 shows much stronger immunity irrelevant to the lower dielectric constant.

The current versus voltage (*I*−*V*) of SiNWs with O (Figure 2a) and OHA (Figure 2b) thin films was measured. The current flow in SiNWs with 150−300 nm width was measured at a bias ranging from −1.5 to 1.5 V using two-terminal of metal electrodes. The measured *I*−*V* curves revealed good ohmic contact property between the Si nanochannel and metal electrode. Also, the current increased with increasing width of the nanochannel.

Figure 3 presents the channel sensitivity depending on the width for different pH buffer solutions of a single O thin film and a staked OHA thin film, respectively. In this experiment, the sensitivity of the SiNW channel is defined as a time-dependent variation in channel current for each pH level. The devices with O or OHA thin films exhibited similar characteristics, namely, the channel current ratio of both devices increase with decreasing channel width. Also, as the pH level increases, the silicon channel surfaces become more negatively charged, which in turn induces accumulation of holes within the p-type nanochannel. As a result, the channel current increases as shown in the insets. It is noteworthy that the output current of the OHA thin film is higher than that of the conventional single O thin film. This is because although both OHA layer and single SiO_2 layer have similar physical oxide thicknesses, the OHA gate dielectric has a thinner equivalent oxide thickness than the single SiO_2 layer because of higher dielectric constants of HfO_2 and Al_2O_3 layers. As a result, a larger capacitance of OHA gate dielectric enlarges the electrical field across the gate dielectric layer.[18] This, in turn, induces a more conductive path in nanowire channel and increases the output current. According to Park et al, the sensitivity of SiNW can be expressed as[19]

$$S = \frac{\Delta G}{G_0} \approx -\frac{(W + 2h)}{Wh}\frac{N_S}{N_A}$$

where *G* is the channel conductance, *W* is the channel width, *h* is the channel height, N_S is the total number of surface sites, and N_A is the channel doping concentration. On the basis of this relationship, it is predicted that the higher N_S contributes to the higher sensitivity. As a result, the SiNW sensors of the OHA thin film reveal higher pH sensitivity (10.80 nA/pH) compared to that of the O thin film (4.83 nA/pH) at a channel of 150 nm-width and 10 μm-length. It means that the Al_2O_3 thin film has a larger number of surface sites than the O thin film.[20]

dx.doi.org/10.1021/am401026z | ACS Appl. Mater. Interfaces 2013, 5, 5214−5218

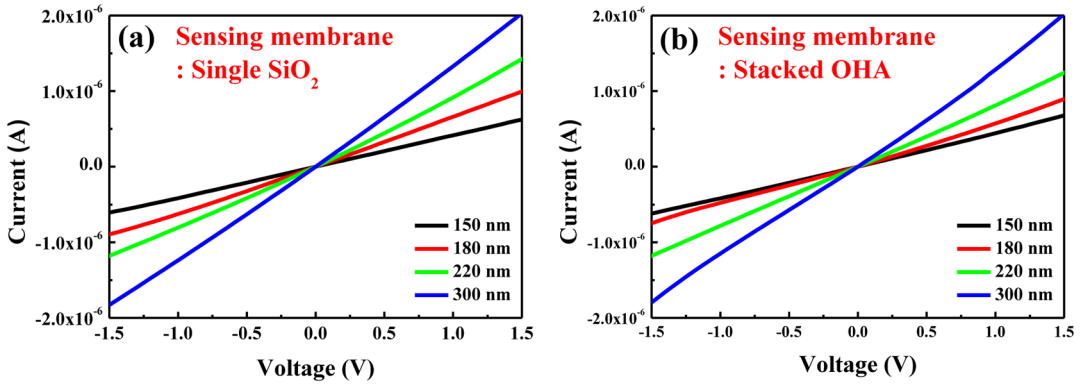

Figure 2. *I*–*V* curves of silicon nanowire depending on the width with (a) single SiO_2 and (b) stacked OHA sensing thin film.

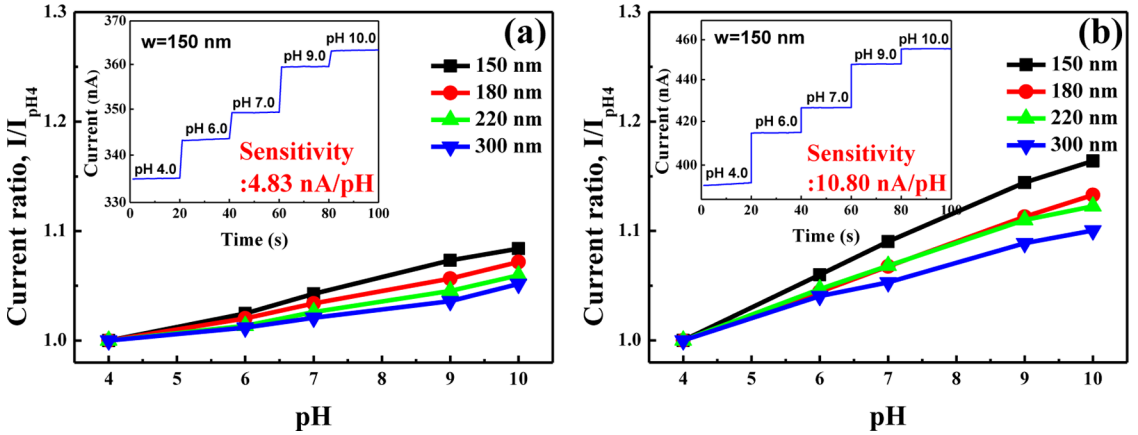

Figure 3. Relative amount of the channel current in different pH of the buffer solutions with (a) single SiO_2 and (b) stacked OHA sensing thin film. The inset shows the real-time response of a 150 nm-wide Si nanochannel.

Figure 4 shows the relation between channel width and pH sensitivity. Obviously, the sensitivity of the OHA thin film is higher than that of the O thin film irrespective of SiNW channel width. Meanwhile, the ratio of sensitivity decreases with increasing channel width. This is because the controllability regarding the current path of the SiNW channel strongly depends on the diameter; the smaller channel diameter, the better field effect on sensitivity at the same doping concentration. In Drude model, assuming uniform current density, the conductance G of a cylindrical wire with radius r (related width) and length l is expressed as[21]

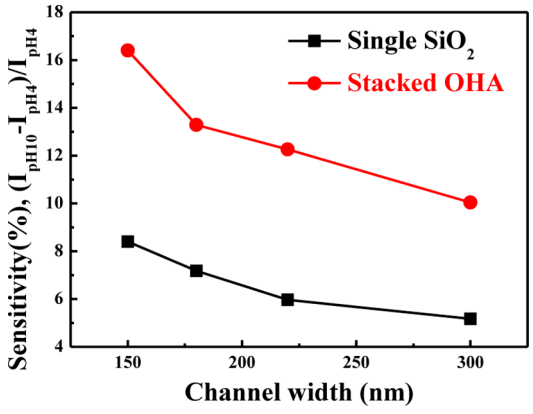

Figure 4. Channel widths versus pH sensitivity for SiO_2 and OHA thin films.

$$G = \frac{\pi r^2}{l} n_e e \mu_e \quad (1)$$

where n_e and μ_e are the electron concentration and mobility. According to

$$n_e = n_0 - \frac{2\alpha N_S}{r} \quad (2)$$

where n_0 is electron concentration before nanowire exposure to target solution and α is the charge transfer coefficient, respectively. Therefore, upon chemisorptions

$$\Delta G/G_0 = \frac{2}{r} \cdot \frac{\alpha N_S}{n_0} \quad (3)$$

Apparently, the obtained $1/r$ relationship resembles the plot in Figure 4 and clearly demonstrates that, as the radius (width) decreases, the nanowire becomes more sensitive to chemical adsorption on the surface.

Figure 5 shows the hysteresis curves (V_H) of the SiNW sensors with O and OHA thin films in the pH loop 7–10–7–4–7. The hysteresis effect is due to the interior sites of the sensing thin film having the ability to react with the ions existing in the pH buffer solution.[10] The hysteresis defined as the channel current difference between the initial and terminal current in the pH loop for the single O thin film and staked OHA thin film were 31.7 and 3.73 nA, respectively.

dx.doi.org/10.1021/am401026z | ACS Appl. Mater. Interfaces 2013, 5, 5214–5218

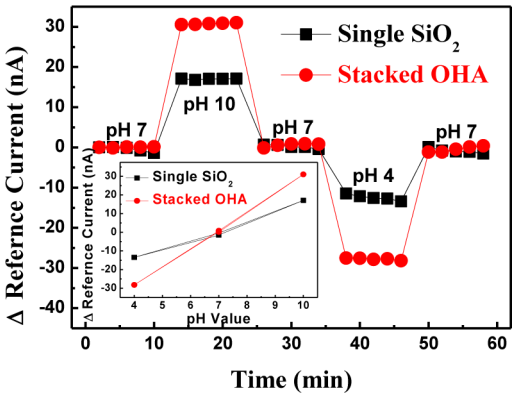

Figure 5. Hysteresis for three buffer solutions with the SiO_2 and OHA sensing thin film. The SiNW sensors were subjected to the pH loop of 7−10−7−4−7 for 60 min. The inset shows the hysteresis widths of each channel current for pH 4, 7, and 10 buffer solutions.

Consequently, the OHA stacked sensing thin film exhibited a smaller hysteresis width than the single O sensing thin film.

Figure 6 displays the drift rate of the different sensing thin films to predict the long-term stability in pH 7 buffer solution

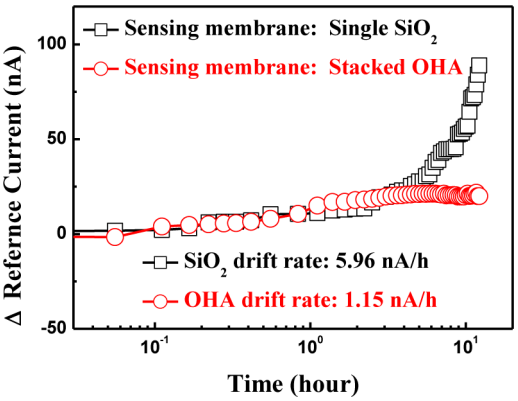

Figure 6. Drift rate in pH 7 buffer solution with the SiO_2 and OHA sensing thin films, for 12 h.

for 12 h. The OHA thin film exhibited more stable drift behavior (1.15 nA/h) than the O thin film (5.96 nA/h). In general, a drift of devices is caused by the slow response site and the buried OH site in sensing thin film. Furthermore, the electrolyte ions can penetrate the hydrated layer of the sensing thin film with increasing measurement time.[22] Then the effective thickness of the gate oxide is decreased, resulting in decreasing threshold voltage with time. Eventually, the drain current of devices increases with time, which induces a problem with the long-term reliability. In particular, the pH solution reacts with the thermally grown SiO_2 layer to form Si−OH sites, leading to a high concentration of nonbridging oxygen sites near the surface, for surfaces exposed to the aqueous electrolyte. On the other hand, the Al_2O_3 layer of the OHA thin film provides endurance as well as improved sensitivity against the hydration during contact with an aqueous solution.[23] To compare with the degrees of degradation for each thin film, variation percentages of V_H and drift rate for the respective sensitivities were extracted. Especially, the OHA thin film revealed the lowest values of 3.73% (V_H variation percentage) and 10.6% (drift rate percentage). As a result, the OHA stacked sensing thin film exhibits excellent characteristics compared with the single O thin film in terms of sensitivity, hysteresis phenomenon, and drift effect as summarized in Table 2.

CONCLUSION

In this work, we realized the SiNW sensors by the "top−down" method using high-k stacked $SiO_2/HfO_2/Al_2O_3$ (OHA) engineered sensing thin films to obtain a higher sensitivity, a stronger chemical immunity, and a better reliability for long-term usage. The sensing characteristics of the engineered OHA thin film were compared with those of the single O thin film. As a result, the OHA thin film revealed higher pH sensitivity compared to the O thin film. Moreover, the output current of SiNW sensors with OHA thin films is higher than that of conventional O thin film owing to a higher dielectric constant. The channel current increased with increasing channel width, but the ratio of sensitivity decreased with increasing channel width due to the controllability of the current path regarding the SiNW channel. The OHA stacked sensing thin films exhibited a smaller V_H in the pH loop 7−10−7−4−7 because the interior sites of the OHA sensing thin film is lower than the single O sensing thin film. The long-term stability predicted by the drift rate revealed that the OHA thin film has more stable drift behavior than the O thin film because the Al_2O_3 of the OHA thin film is more robust to the hydration during contact with an aqueous solution. Accordingly, the SiNW sensors with OHA sensing thin films are expected to be a promising sensor structure for detecting the biological and chemical species with an ultrahigh sensitive, label-free, real-time detection, and CMOS compatibility.

AUTHOR INFORMATION

Corresponding Author

*E-mail address: chowj@kw.ac.kr.

Notes

The authors declare no competing financial interest.

ACKNOWLEDGMENTS

This research was supported by a research grant from Kwangwoon University in 2013, and by the Converging Research Center funded by the Ministry of Education, Science and Technology (No. 2012K001352).

REFERENCES

(1) Quitoriano, N. J.; Kamins, T. I. *Nano Lett.* **2008**, *8*, 4410−4414.
(2) Elfstrom, N.; Linnros, J. *J. Phys.: Conf. Ser.* **2008**, *100*, 052042.
(3) Hernandez, F. J.; Ozalp, V. C. *Biosensors* **2012**, *2*, 1−14.
(4) Baek, D. J.; Duarte, J. P.; Moon, D. I.; Kim, C. H.; Ahn, J. H. *Appl. Phys. Lett.* **2012**, *100*, 213703.

Table 2. Sensing Properties of the SiNW pH Sensors with the O and OHA Sensing Thin Films

sensing thin film	sensitivity (nA/pH)	linearity (%)	V_H (nA)	drift rate (nA/h)	V_H for sensitivity (%)	drift rate for sensitivity (%)
single SiO_2	4.83	99.51	1.53	5.96	31.7	123.4
stacked OHA	10.80	99.51	0.4	1.15	3.73	10.6

(5) Park, C. W.; Ahn, C. G.; Yang, J. H.; Baek, I. B.; Ah, C. S.; Kim, A.; Kim, T. Y.; Sung, G. Y. *Nanotechnology* **2009**, *20*, 475501.
(6) Hahm, J. I.; Lieber, C. M. *Nano Lett.* **2004**, *4*, 51−54.
(7) Kim, A.; Ah, C. S.; Yu, H. Y.; Yang, J. H.; Baek, I. B. *Appl. Phys. Lett.* **2007**, *91*, 103901.
(8) Klemic, J. F.; Stern, E.; Reed, M. A. *Nat. Biotechnol.* **2001**, *19*, 924−925.
(9) Elfstroms, N.; Juhasz, R.; Sychugov, I.; Engfeldt, T.; Karlstrom, A. E.; Linnros, J. *Nano Lett.* **2007**, *7*, 2608−2612.
(10) Bousse, L.; Bergveld, P. *Sens. Actuators, B.* **1984**, *6*, 65−78.
(11) Chou, J. C.; Weng, C. Y. *Mater. Chem. Phys.* **2001**, *71*, 120−124.
(12) Pan, T. M.; Lin, J. C.; Wu, M. H.; Lai, C. S. *Sens. Actuators, B.* **2009**, *138*, 619−624.
(13) Lu, T. F.; Wang, J. C.; Yang, C. M.; Chang, C. P.; Ho, K. I.; Ai, C. F.; Lai, C. S. *Microelectron. Reliab.* **2010**, *50*, 742−746.
(14) Ngai, T.; Qi, W. J.; Sharma, R.; Fretwell, J.; Chen, X. *Appl. Phys. Lett.* **2000**, *76*, 502−504.
(15) Lin, Y. S.; Puthenkovilakam, R.; Chang, J. P. *Appl. Phys. Lett.* **2002**, *81*, 2041−2043.
(16) Pan, T. M.; Huang, M. D.; Lin, C. W.; Wu, M. H. *Sens. Actuators, B.* **2010**, *144*, 139−145.
(17) Schoning, M. J.; Mourzina, Y. G.; Schubert, J.; Zander, W.; Legin, A.; Vlasov, Y. G.; Luth, H. *Sens. Actuators, B.* **2001**, *78*, 273−278.
(18) Robertson, J.; Falabretti, B. *Mater. Sci. Eng., B.* **2006**, *135*, 267−271.
(19) Park, I.; Li, Z.; Li, X.; Pisano, A. P.; Williams, R. S. *Biosens. Bioelectron.* **2007**, *22*, 2065−2070.
(20) Bergveld, P. *Sens. Actuators, B.* **2003**, *88*, 1−20.
(21) Fan, Z.; Lu, J. G. *IEEE Trans. Nanotechol.* **2006**, *5*, 393−396.
(22) Jamasb, S.; Collins, S.; Smith, R. L. *Sens. Actuators, B.* **1998**, *49*, 146−155.
(23) Matsuo, T.; Esashi, M. *Sens. Actuators, B.* **1981**, *1*, 77−96.